*IET Power Electronics*

WILEY

The Institution of Engineering and Technology

ORIGINAL RESEARCH OPEN ACCESS

# Direct Voltage Measurement for Sensorless Control of Single-Stage Current Source Inverter in Motor Drive Applications

Emilio Carfagna[1] | Giovanni Migliazza[1] | Giampaolo Buticchi[2] | Emilio Lorenzani[1,3]

[1]Department of Science and Methods for Engineering, University of Modena and Reggio Emilia, Reggio Emilia, Italy | [2]Key Laboratory of More Electric Aircraft Technology of Zhejiang Province, University of Nottingham Ningbo China, Ningbo, China | [3]InterMech–MO.RE., University of Modena and Reggio Emilia, Modena, Italy

**Correspondence:** Giovanni Migliazza (giovanni.migliazza@unimore.it)

**Received:** 19 August 2025 | **Revised:** 28 October 2025 | **Accepted:** 9 November 2025

## ABSTRACT

Current source inverters (CSIs) offer an alternative to voltage source inverters (VSIs) for electric motor applications. CSIs have some advantageous characteristics, such as the ability to inherently boost voltage, the absence of electrolytic capacitors, and reduced voltage stress on the machine. However, the increased component count and the need for a pre-stage to control the inductor current have limited the adoption of CSIs. For applications that must operate above a base speed, such as more electric aircraft (MEA), single-stage CSI converters are a promising solution. The ability to directly measure the terminal voltages allows for a simple and robust sensorless control approach to be used with this power converter. This approach based on a phase-locked loop (PLL) directly connected to the voltages with a feedforward compensation that depends on voltage drops on Rs and L0 is compared against a back-EMF (BEMF) observer. If a machine with an anisotropic rotor is used and the impedance is small, the feedforward compensation can be neglected leading to the classical PLL. Experimental results on a CSI7 converter driving a permanent magnet synchronous machine (PMSM) report that this kind of sensorless control can be a suitable alternative in motor drive applications.

## 1 | Introduction

Variable-speed drives (VSDs) are usually based on the well known voltage-source inverter (VSI) topology, due to its simplicity and efficiency. On the other hand, current source inverter (CSI) needs reverse-voltage blocking (RVB) switches and, historically, during the 1960s and 1970s, thyristors and gate turn-off thyristors were used [1]. CSI based on thyristor is still used for particularly high-power (in the order of MW) slow-dynamic applications. For example, in [2] the proposed converter configuration uses a thyristor-based CSI drive with parallel installation of the VSI and the capacitor to manage the reactive power, with an improved harmonic spectrum, while [3] deals with the case of an induction motor drive with open-end stator winding with the CSI connected at one side of the stator winding and a capacitor fed-VSI at the other end. Furthermore, CSI needs a constant current source, which is typically obtained with a pre-stage, containing a bulky inductor. The pre-stage converter can be a current source rectifier (CSR) [4] with AC voltages, where as in case of DC voltages a bidirectional chopper [5] or a full bridge [6] are adopted.

The advent of wide-bandgap (WBG) bi-directional switches poses critical questions when using them in VSI [7], reopening the field for CSI with improved efficiency. In fact, as shown in [8], for an electric drive based on CSI the weight and volume of the power converter is higher then an equivalent VSI, but the size of the electric motor results lower. For these reasons, in particular applications like more electric aircraft (MEA) [9] and more electric propulsion (MEP) [10] the CSI represent a competitive design choice at the system level. This is of interest in applications

with higher operational speeds that provide traction power for electric propulsion in railways (see [11] for the lifetime evaluation of power devices), ships (see [12] for hardware in the loop emulation for marine vessels) and electric vehicles (see [13] for the control of a ultrahigh-speed machine as air compressor in fuel cell vehicles). Furthermore, CSI has several advantages over VSI, in terms of filtered output voltages that reduces the voltage stress on the machine, reduced electromagnetic interference (EMI), reliability and fault-tolerance [14]. A review on the advantages of the CSI considering different architectures and switching devices is reported in [15].

For applications where the converter needs to operate above a base speed (e.g., for compressors and fans) the use of the single-stage CSI (i.e., CSI without pre-stage converter) can be unlocked. In this way the inductor current control is performed using the modulation index [16] and a compact, robust and efficient solution for a CSI drive can be realized, despite some drawbacks like the necessity to have a back electromotive force (back-EMF) higher than the DC input voltage, which prevents continuous operations at lower rotational speed. This issue is discussed in [17] that adds a parallel discharge path to extend the operating region of the converter down to zero speed.

The use of position sensors (like encoders or resolvers) is difficult in different industrial environments due to the presence of high temperature, dust or vibrations and it is well-known that the most common sensorless algorithms for synchronous machines with VSI can be divided into model-based (like stator flux observers [18], linear back-EMF observers [19], sliding mode observers [20], extended Kalman filters [21]) and frequency signal injection (like high frequency [22] or low frequency [23]). The frequency injection is effective only at standstill and in low speed region, as studied by [22], while [24] extends the high frequency injection in case of unbalanced output capacitors. It is also possible to merge model-based observers and frequency injection as in [25].

Employing a CSI-fed permanent magnet synchronous machine (PMSM), a sensorless control has been proposed in [26] using sliding mode observer with frequency-locked loop (FLL), whereas [27] deals with the case of long cable connections. The same problem with long cables is studied in [28] for an induction machine. In [29] a smooth transition between I-f startup and closed loop field oriented sensorless control is studied. Practical implementation issues of model-based observers for CSI-fed PMSM such as offset errors, discretization and measurement noises are discussed in [30]. Model-based observers rely on the back-EMF constant $k_{\mathrm{M}}$ (equal to $p\Phi_{\mathrm{PM}}$ where $p$ is the number of poles pairs and $\Phi_{\mathrm{PM}}$ is the flux linkage provided by the permanent magnet), on the stator inductance $L_0$ and on the stator resistance $R_s$ that are usually identified with sufficient model information, but the well-known rank-deficient and ill-convergence problem in $dq$ reference frame limits the performances of this approach [31]. A common solution with this problem, is fixing some of these parameters reducing the number of parameters to be identified [32]. An alternative is a proper injection of an high frequency current [33], but this additional current affect the current control performance and uses additional voltage injection. On the other hand, to overcome the rank deficiency problem, the parameters estimation is performed in the fixed reference frame using a recursive least squares algorithm [34], while [35] solves the same problem using current derivative to avoid the rank-deficiency issues.

An additional advantage, not yet explored, is that the CSI allows for a direct measurement of the motor terminal voltages, enabling an easy and robust sensorless control. In fact, the sensorless schemes exposed before need a model-based observer to extract information about the position from the stator fluxes or the back-EMF and a phase-locked loop (PLL) is added to extract information about the speed. Using a VSI, the voltages computed by the control are adopted for the model-based observer because the output voltages need a strong filtering action. This issue is solved with CSI because the output capacitor $C_f$ filter the high-frequency components of the currents ensuring a quasi-sinusoidal behavior of the voltages. In this way it is possible to directly extract information about position/speed with a PLL that does not rely on the electrical parameter of the machine.

A preliminary analysis has been carried out in [36] by means of numerical simulations, in this paper it will be experimentally shown how a PLL can achieve good performance without the knowledge of the machine parameters. This fact solves the common issue of stator flux and back-EMF observers that suffers from wrong knowledge of the electrical parameters, in particular $L_0$ [37] in high speed region, whereas in low speed region the observers are more sensible to $R_s$ errors [38] and to dead-time of the power devices [39].

In this work, a PLL structure is used to extract information about rotor position/speed directly from the voltage measurement. This control strategy is compared against a back-EMF (BEMF) observer commonly used for sensorless control with VSI and analyzed in [19]. This observer has a Luenberger structure with a linear correction, differently from [26] and [27] that use a BEMF observer with the correction performed using sliding mode control with sigmoidal functions. Table 1 summarizes the adopted sensorless schemes used for CSI topologies. The control strategies based on high frequency injection are effective only at standstill and in low speed region, while the aim of the proposed approach takes into account the case of anisotropic rotor with small impedance in high speed region.

The paper is organized as follows: Section 2 summarizes the peculiarities of single-stage CSI7 topology with DC-link current control, while Section 3 deals with the classical sensorless control with back-EMF observer commonly used with VSI topology and the proposed sensorless scheme based on the direct measures of the output voltages. Section 4 verifies the strategies with experimental test, followed by conclusions in Section 5.

## 2 | Single-Stage Current Source Inverter CSI7

The power converter known as CSI7 is proposed in [40] and reported in Figure 1. The converter comprises seven RVB switches in a three-phase full-bridge configuration with the presence of the capacitive output filter $C_f$ with the aim of filter the high frequency components of the modulated currents. As alternative to the output capacitor filters, in [41] a three-level converter is used as an active filter.

**TABLE 1** | CSI architectures with sensorless control schemes used in the state-of-the-art.

| Sensorless | Hardware topology | Control architecture | Order |
|---|---|---|---|
| [22] | CSI with rectifier | High-frequency injection + PLL | 2 (Bandpass filter) + 1 (Low pass filter) + 2 (PLL) |
| [24] | CSI with rectifier | High-frequency injection + PLL | 1 (Low pass filter) + 2 (PLL) |
| [26] | CSI with rectifier | Observer + PLL | 4 (BEMF observer) + 2 (PLL) |
| [27] | CSI with rectifier | Observer + PLL | 4 (BEMF observer) + 2 (PLL) |
| [28] | CSI with rectifier | Observer + PLL | 2 (Stator model) 2 (Rotor model) + 2 (PLL) |
| [29] | CSI with rectifier | Observer + PLL | 4 (BEMF observer) + 2 (PLL) |
| [36] | Single-stage CSI | Observer + PLL PLL | 4 (BEMF observer) + 2 (PLL) 2 (only PLL) |
| Proposed | Single-stage CSI | PLL | 2 (PLL) |

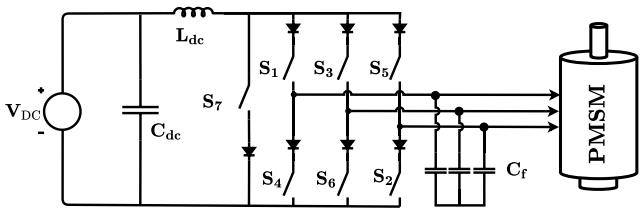


**FIGURE 1** | Schematic of a single-stage CSI7 topology with a PMSM as load.

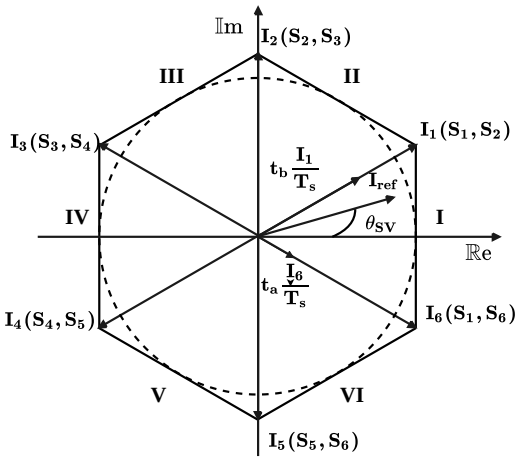


**FIGURE 2** | Space vector modulation for CSI.

The working principle of the CSI assumes that a constant current source is available. Common passive diodes configurations or other setups [5, 6] that are commonly adopted to implement a pre-stage converter able to guarantee a proper DC current which has always been a defining challenge of the CSI. The key idea exposed in [16] is that for a single-stage CSI the modulation index is able to control the output currents and the DC-link current $i_{dc}$ without a pre-stage converter.

In Figure 2, the modulation index $m$ is defined as

$$m = \frac{|\mathbf{I}_{ref}|}{i_{dc}}, \tag{1}$$

where $\mathbf{I}_{ref}$ is the output current vector. The maximum value of $\mathbf{I}_{ref}$ corresponds to the maximum radius of the circle that can be inscribed into the hexagon, namely $i_{dc}$. The modulation index is in the range $[0, 1]$.

The principle of the SVM is the capability to choose how to synthesize $\mathbf{I}_{ref}$ by selecting the best combination of active and zero vectors. Different combination of on-switches, referred as states, are used. During active states on-switches are in diagonal (e.g., $S_1$ and $S_6$), allowing the DC-current to flow to the load, while during zero state on-switch is on $S_7$ and the DC-current is not transferred to the load charging the inductor $L_{dc}$. Any output current vector $\mathbf{I}_{ref}$ in a sextant of the hexagon can be generated by a time-weighted linear combination of the two active vectors, $\mathbf{I}_a$ and $\mathbf{I}_b$, and the zero vector $\mathbf{I}_z$ as

$$\mathbf{I}_{ref} T_s = \mathbf{I}_a t_a + \mathbf{I}_b t_b + \mathbf{I}_z t_z, \tag{2}$$

where $t_a$, $t_b$ and $t_z$ are the dwell times, respectively, of the current vectors $\mathbf{I}_a$, $\mathbf{I}_b$ and $\mathbf{I}_z$. The dwell times are constrained in a switching time period $T_s$, thus $T_s = t_a + t_b + t_z$. During the transition between two vectors, an overlapping time where two vectors are applied simultaneously is introduced to prevent the open-load condition that would create an over voltage due to the inductive DC link gives rise to a potential devices creeping. The values of the active states A/B are given by $t_a$ and $t_b$ described by $d_a T_s$ and $d_b T_s$, respectively. The dwell times intervals of the two active states and of the zero state are

$$\begin{cases} t_a = m \sin\left(\frac{\pi}{6} - \theta_{SV}\right) T_s \\ t_b = m \sin\left(\frac{\pi}{6} + \theta_{SV}\right) T_s \\ t_z = T_s - t_a - t_b \end{cases} \tag{3}$$

where $\theta_{SV}$ is the angle between $\mathbf{I}_{ref}$ and the bisector of the sextant in which $\mathbf{I}_{ref}$ is located. The term $\theta_{SV}$ is computed as $\theta - (\mathrm{k} - 1)\pi/3$ (where $k$ is the sextant in Figure 2), thus $\theta_{SV} \in [-\pi/6, \pi/6]$.

## 3 | Sensorless Control Strategies

This section introduces the Observers that will be compared in the Experimental Section. In particular are hereby analyzed: the classical linear back-EMF observer [19] and the proposed

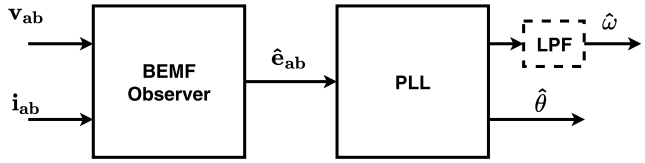


**FIGURE 3** | Sensorless structure with back-EMF observer and phase-locked loop (PLL).

sensorless scheme based on quadrature PLL enforced with feedforward compensation.

### 3.1 | Classical Linear Back-EMF Observer

The control strategy is shown in Figure 3. Considering the back-EMF terms $e_a$ and $e_b$:

$$\begin{cases} e_a = -k_M \omega \sin(p\theta) \\ e_b = k_M \omega \cos(p\theta) \end{cases} \tag{4}$$

where $\theta$ is the (mechanical) rotor angle, $\omega$ is the (mechanical) rotor speed, the dynamical model of the electrical part can be written as:

$$\begin{cases} \dfrac{di_a}{dt} = -\dfrac{R_s}{L_0} i_a + \dfrac{1}{L_0}(u_a - e_a) \\ \dfrac{di_b}{dt} = -\dfrac{R_s}{L_0} i_b + \dfrac{1}{L_0}(u_b - e_b) \\ \dfrac{de_a}{dt} = -p\omega e_b + p e_a \dfrac{d\omega}{dt} \\ \dfrac{de_b}{dt} = p\omega e_a + p e_b \dfrac{d\omega}{dt} \end{cases} \tag{5}$$

where $(i_a, i_b)$ are the stator currents, $(u_a, u_b)$ are the stator voltages.

Assuming that the rotor speed $\omega$ is slowly varying respect to the electrical quantities, it follows that $\omega$ and its derivative can be neglected from the electrical model

$$\begin{cases} \dfrac{de_a}{dt} \simeq 0 \\ \dfrac{de_b}{dt} \simeq 0 \end{cases} \tag{6}$$

So a classical Luenberger structure can be constructed as in [19]:

$$\begin{cases} \dfrac{d\hat{i}_a}{dt} = -\dfrac{R_s}{L_0} i_a + \dfrac{1}{L_0}(u_a - \hat{e}_a) + k_i(i_a - \hat{i}_a) \\ \dfrac{d\hat{i}_b}{dt} = -\dfrac{R_s}{L_0} i_b + \dfrac{1}{L_0}(u_b - \hat{e}_b) + k_i(i_b - \hat{i}_b) \\ \dfrac{d\hat{e}_a}{dt} = -k_e(i_a - \hat{i}_a) \\ \dfrac{d\hat{e}_b}{dt} = -k_e(i_b - \hat{i}_b). \end{cases} \tag{7}$$

with $(\hat{i}_a, \hat{i}_b)$ being the estimated currents, $(\hat{e}_a, \hat{e}_b)$ the estimated back-EMF and $k_i$, $k_e$ positive gains of the observer. Introducing the estimation errors $\tilde{i}_a = i_a - \hat{i}_a$, $\tilde{i}_b = i_b - \hat{i}_b$, $\tilde{e}_a = e_a - \hat{e}_a$ and $\tilde{e}_b = e_b - \hat{e}_b$ the back EMF observer leads to the following linear dynamic for the estimation error:

$$\frac{d}{dt}\begin{bmatrix} \tilde{i}_a \\ \tilde{i}_b \\ \tilde{e}_a \\ \tilde{e}_b \end{bmatrix} = \begin{bmatrix} -k_i & 0 & -\dfrac{1}{L_0} & 0 \\ 0 & -k_i & 0 & -\dfrac{1}{L_0} \\ k_e & 0 & 0 & 0 \\ 0 & k_e & 0 & 0 \end{bmatrix} \begin{bmatrix} \tilde{i}_a \\ \tilde{i}_b \\ \tilde{e}_a \\ \tilde{e}_b \end{bmatrix} \tag{8}$$

The estimation error tends to zero when a proper choice of the observer gains $k_i$ and $k_e$ is used through a linear pole-placement technique.

The choice of the poles determines the dynamics of the estimation error cancellation. It must be sufficiently fast compared to the dynamics of the state variables, and it must be sufficiently slow in order to attenuate the measurement noise.

The transfer function linking the estimated and actual back-EMFs can be computed from (5) and (7) using the Laplace variable $s$:

$$\frac{\hat{E}_{ab}}{E_{ab}}(s) = \frac{k_e}{L_0 s^2 + k_i L_0 s + k_e} \tag{9}$$

The result is a common second order low pass filter with natural frequency $\omega_n$ equal to $\sqrt{k_e/L_0}$ and damping factor $\zeta$ equal to $k_i/(2\omega_n)$ that can be used to tune the observer's gains $k_i$ and $k_e$.

### 3.2 | Quadrature Phase-Locked Loop (PLL) With Feedforward Compensation

The use of a sensorless control approach can improve the robustness of the drive and eliminate the need for a position/speed sensor. With a VSI, measuring the motor terminals requires either a low-pass filter to remove PWM harmonics or an estimation based on the duty cycle that suffer from dead-time of the devices [39]. The unique characteristics of the CSI converter make it well-suited for implementing this type of control. The key feature of the CSI converter is the presence of a capacitive output filter. This filter significantly reduces voltage distortion at the machine terminals, enabling direct voltage measurement using voltage sensors ensuring a fast and precise estimation of the equivalent voltage phasor.

A PLL can be utilized for this purpose [42]. By measuring the phase voltages, a standard three-phase PLL with a very fast dynamic response can be developed. The advantage of directly estimating the voltage terminal phasor is that a very wide bandwidth can be achieved, as no integral operations are required to evaluate the flux.

Figure 4 shows the overall block diagram of the PLL with angle compensation. A phase displacement of $-\pi/2$ is added to the PLL angle to re-synchronize with the most common field-oriented

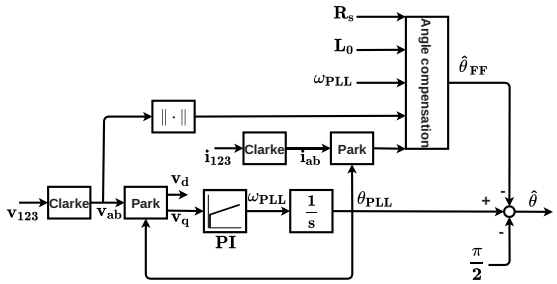


**FIGURE 4** | PLL structure with feedforward angle compensation.

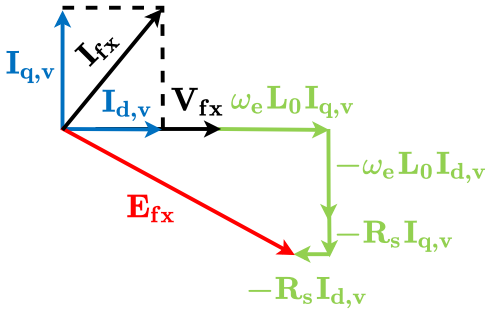


**FIGURE 5** | Phasor diagram of the terminal voltage with the resistive and inductive voltage drops.

control scheme. This estimated angle is used as the reference angle for the field oriented control.

By the way, the terminal voltage phasor differs from the back-EMF phasor due to the voltage drops across the phase resistance and inductance. One possible solution would be to subtract the resistive and inductive voltage drops from the terminal voltage before feeding it into the PLL, but calculating the derivative of the motor current would introduce unacceptable issues related to noise.

A better solution is to use a feed-forward compensation of the voltage drops, by leveraging the phasor equations.

Figure 5 shows the terminal voltage phasor along with the $dq$ components of the current and the voltage drops. The phase back-EMF can be computed as in (10):

$$E_{fx} = V_{fx} - R_s I_{fx} - j\omega_e L_0 I_{fx} \tag{10}$$

The angle error between the back-EMF phasor and the terminal voltage can be calculated through the relationship:

$$\theta_{FF} = \arctan\left(\frac{\omega_e L_0 I_{d,v} + R_s I_{q,v}}{V_f - R_s I_{d,v} + \omega_e L_0 I_{q,v}}\right) \tag{11}$$

In case of a PMSM with an anisotropic rotor, the equation needs to be changed to account for the difference in the inductance. However, it is worth noticing that the angle compensation can be neglected if the impedance of the machine is small and the field oriented control is performed using the reference current $i_d^\star$ equal to zero. In this case, there is no longer the need to perform an inverse tangent operation in real-time. With this approximation,

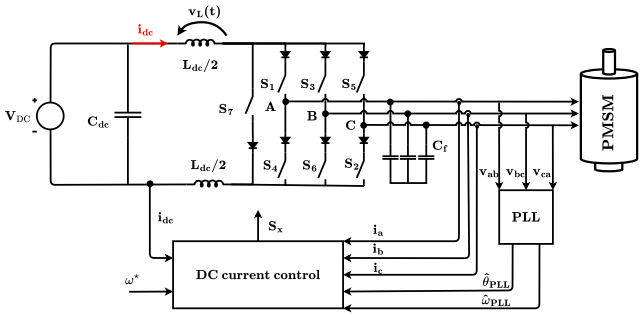


**FIGURE 6** | Control strategy with quadrature PLL.

**TABLE 2** | Current source inverter parameters.

| Name | Symbol | Value | Unit |
|---|---|---|---|
| DC voltage | $V_{DC}$ | 50 | V |
| Input inductance | $L_{dc}$ | 2 | mH |
| Sampling time | $T_s$ | 100 | μs |
| Overlap time | $T_{ov}$ | 1 | μs |
| Output filter capacitor | $C_f$ | 2.2 | μF |

**TABLE 3** | PMSM parameters.

| Name | Symbol | Value | Unit |
|---|---|---|---|
| Nominal phase current | $I_N$ | 16.4 | $A_{pk}$ |
| Fundamental frequency | $f_N$ | 166.6 | Hz |
| Nominal speed | $n_N$ | 2500 | rpm |
| Stator resistance | $R_s$ | 0.35 | Ω |
| Synchronous inductance | $L_0$ | 1.7 | mH |
| Back-EMF constant | $k_M$ | 0.8884 | V s/rad |
| Poles pair | $p$ | 4 | — |

the transfer function of the PLL is equal to

$$PLL(s) = \frac{k_p s + k_i}{s^2 + k_p s + k_i} \tag{12}$$

where $k_p$ and $k_i$ are the proportional and integral parameters of the PI regulator in Figure 4. For the observer of Section 3.1, this transfer function is connected in series to back-EMF observer. The full control strategy is shown in Figure 6.

## 4 | Experimental Results

The main parameters of the CSI7 converter and of the PMSM are reported in Tables 2 and 3, respectively. The CSI7 is connected to a PMSM machine as shown in Figure 7. A machine with limited speed is used, and an input voltage of 50 V as the DC bus is selected. The prototype system has been developed based on SiC devices. A commercial TMS320F2812 digital signal controller that implements the modulation strategy and the control with a sampling and switching frequency of 10 kHz was used. The

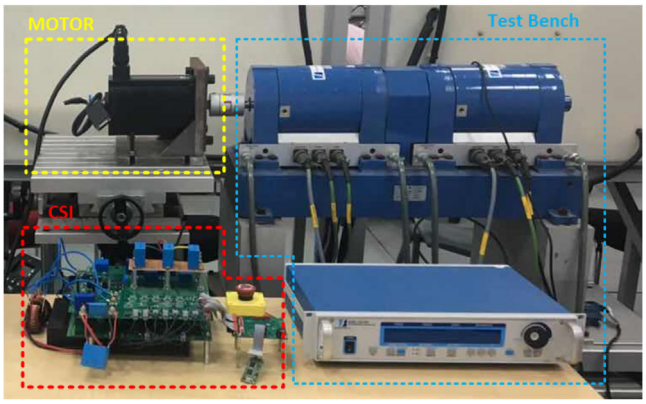


**FIGURE 7** | Single-stage CSI7 with SiC devices and test bench.

proposed sensorless control strategy in Section 3.2 is compared to the back-EMF observer of [19], summarized in Section 3.1.

To allow a sensorless scheme, voltage sensors are adopted in order to measure the terminal voltages. Differently from VSIs that adopt the reference voltages in sensorless schemes due to the difficulty of filtering the measured ones without introducing significant lags, with CSIs it is simple to have smoother signals due to the presence of capacitor filters at the CSI output.

Having set up the prototype and its test bench, a series of experimental runs were designed to prove the concept of the proposed schemes and also investigate its stability when various operating conditions are considered.

Figure 8 shows the experimental results when the PMSM is driven from 1000 rpm to 2500 rpm (with intermediate steps of 500 rpm applied every 3 s) under a constant load torque of 1 Nm. It is worth noting that the speed tracking (in the top figure) is ensured for every control strategy and the waveform of $i_{dc}$ have the same behavior.

Figure 9 reports the experimental results when the PMSM is driven at constant speed of 1000 rpm under a variable load torque from 0 Nm to 6 Nm (with intermediate steps of 2 Nm). It can be seen that the speed tracking is maintained for every control strategy and $i_{dc}$ have the same waveform.

The RMS currents of $i_a$ and the mean current of $i_{dc}$ are evaluated with errors based on knowledge of $R_s$ and $L_0$ in steady state conditions with a speed reference of 1500 rpm and a load torque of 3 Nm. From Table 4, it can be seen that the solutions with PLL have a higher value of the RMS current on the DC link, while the RMS current on $i_a$ has a degradation if $L_0$ is higher respect to the nominal one. The parameters are modified in the implementation of the back-EMF observer of (7). It can be noted that the RMS errors on $R_s$ have smaller influence, while the impact of $L_0$ for this kind of observer needs to be taken into account because in case of heavily saturated machines the value of the inductance of the PMSM is strongly reduced. From Figure 10, it can be seen that the sinusoidal shape of the output current is ensured for every observer.

**TABLE 4** | RMS values of the sensorless strategies with speed reference of 1500 rpm with 3 Nm of load torque.

| | $i_a$ RMS [$A_{RMS}$] | $i_{dc}$ Mean [A] |
|---|---|---|
| Control with sensor | 2.21 | 14.08 |
| BEMF nominal | 2.25 | 14.10 |
| BEMF +50% $R_s$ | 2.27 | 14.19 |
| BEMF −50% $Rs$ | 2.28 | 14.21 |
| BEMF +60% $L_0$ | 2.40 | 14.27 |
| BEMF −60% $L_0$ | 2.25 | 14.20 |
| PLL with feedforward | 2.26 | 14.33 |
| PLL | 2.26 | 14.36 |

**TABLE 5** | Computational cost of implemented strategies.

| Strategy | Computational cost [μs] |
|---|---|
| Control with sensor | 10.55 |
| BEMF with PLL | 30.04 |
| PLL with feedforward | 31.08 |
| PLL | 23.72 |

In Figure 11, the effect of the feedforward compensation proposed in (11) is discussed. The motor follows a reference of 1000 rpm at no load condition and a load torque of 6 Nm is applied. It can be seen that the value of the feedforward compensation is limited around 0° even in transient condition. The same situation appears even in case of constant torque with variable reference speed.

From the experimental results, it is reported that using a machine with anisotropic rotor and small impedance in high speed region, it is possible to obtain a simple sensorless control with a direct measure of the output voltages without any knowledge of the electrical parameters of the machine, leading to an inherently robustness of the control.

### 4.1 | Computational Cost

The computational cost of the three strategies is compared based on the execution times when the control is closed on the speed loop. The algorithms runs with an internal clock of 80 MHz and results are summarized in Table 5.

Due to the evaluation of sinusoidal and co-sinusoidal functions to compute the feedforward, the execution time of the proposed compensation is bigger respect to the other strategies.

## 5 | Conclusion

This paper introduces a sensorless control approach for a current source inverter (CSI) used as a single-stage variable speed drive.

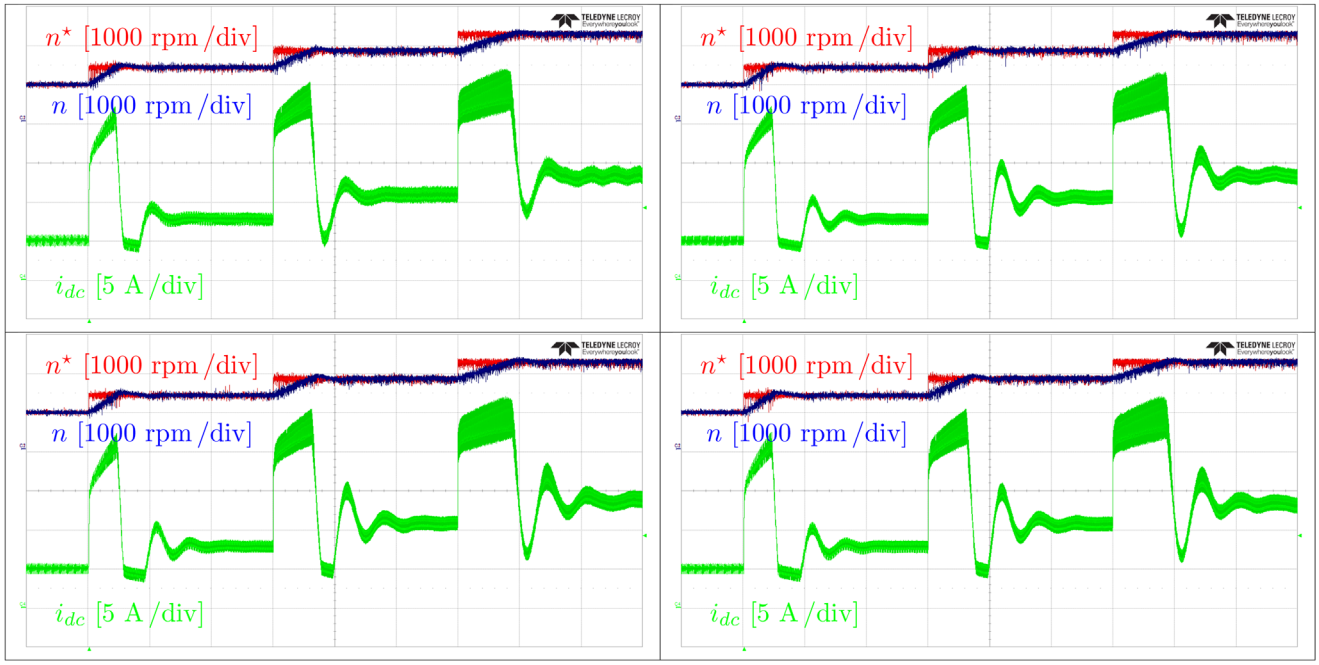


**FIGURE 8** | First row from left to right: control with sensor; sensorless control with back-EMF observer. Second row from left to right: sensorless control with PLL with feedforward, sensorless control with PLL. Speed step from 1000 rpm to 2500 rpm with intermediate steps of 500 rpm and constant torque of 1 Nm. Red trace: speed reference, blue trace: measured speed, green trace: measured $i_{dc}$ current (5 A/div). The time division is 1 s/div.

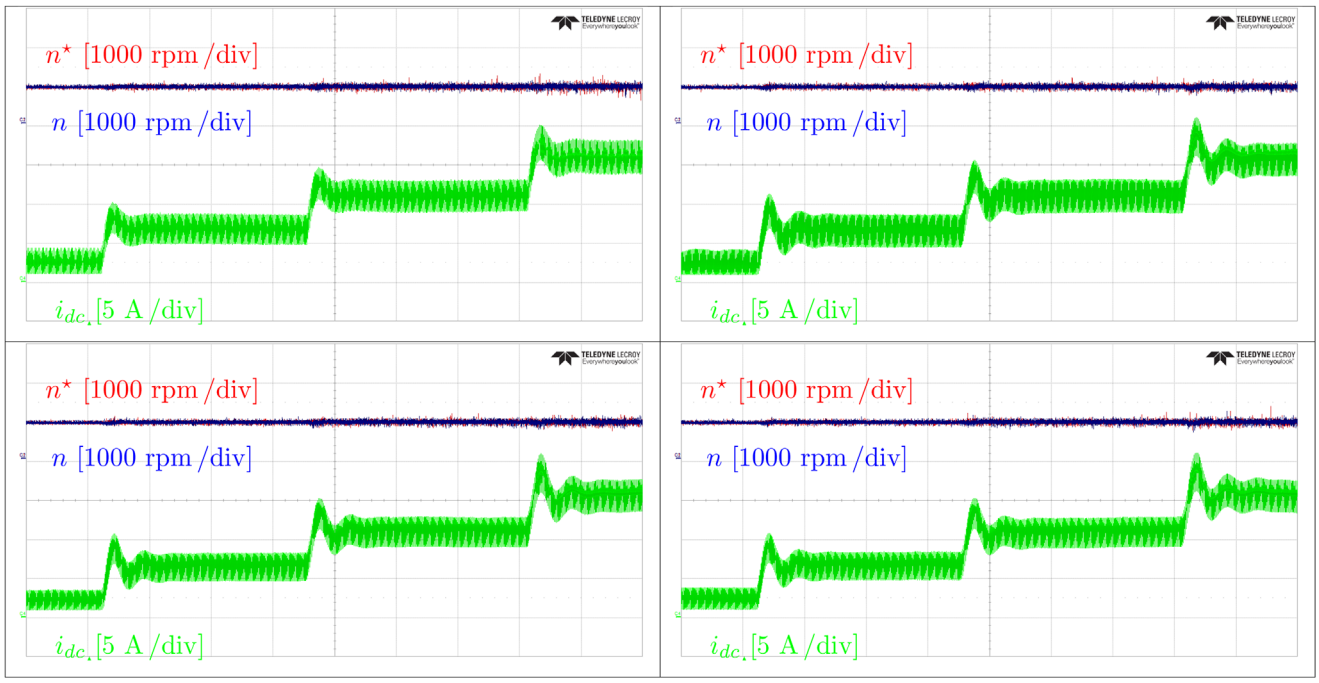


**FIGURE 9** | First row from left to right: control with sensor; sensorless control with back-EMF observer. Second row from left to right: sensorless control with PLL with feedforward, sensorless control with PLL. Load step from 0 Nm to 6 Nm with intermediate steps of 2 Nm and constant speed reference of 1000 rpm. Red trace: speed reference, blue trace: measured speed, green trace: measured $i_{dc}$ current (5 A/div). The time division is 1 s/div.

The key aspect of the proposed method is the direct availability of the motor terminal voltage, which enables the direct adoption of a PLL for estimating the rotor angle. Different sensorless control strategies are evaluated, and the results demonstrate that the proposed solution is competitive with the state-of-the-art approaches while still delivering satisfactory performance. It has been shown that if a PMSM with anisotropic rotor is adopted, the feedforward compensation can be removed leading to satisfactory results even without prior knowledge of the machine and load parameters, thereby ensuring inherent robustness. Furthermore, the computational cost is reduced without the use of additional observer structures.

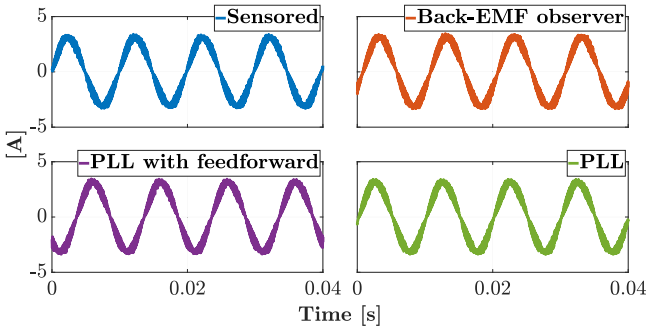


**FIGURE 10** | Output current $i_a$ with reference of 1500 rpm and 3 Nm of load torque. The blue trace is the output current for sensored control and the other traces are the output currents for every observer (orange for back-EMF observer, purple for PLL with feedforward and green for PLL).

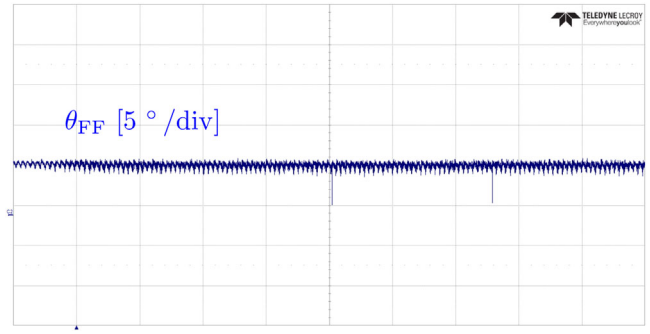


**FIGURE 11** | PLL with feedforward: load step from 0 Nm to 6 Nm with constant speed of 1000 rpm. Blue trace: feedforward angle compensation (5°/div). The time division is 200 ms/div.

### Author Contributions

**Emilio Carfagna:** methodology, software, validation, investigation, data curation, writing – original draft preparation, writing – review and editing. **Giovanni Migliazza:** methodology, software, validation, investigation. **Giampaolo Buticchi:** conceptualization, methodology, supervision, writing – review and editing. **Emilio Lorenzani:** supervision, writing – original draft preparation, writing – review and editing, supervision. All authors have read and agreed to the published version of the manuscript.

### Funding

This study was supported by NextGenerationEU (Grant No. 0001052).

### Conflicts of Interest

The authors declare no conflicts of interest.

### Data Availability Statement

The authors elect to not share data.

### References

1. B. Wu and M. Narimani, *High-Power Converters and AC Drives*, Vol. 59 (John Wiley & Sons, 2017).

2. S. Kwak and T. Kim, "An Integrated Current Source Inverter With Reactive and Harmonic Power Compensators," *IEEE Transactions on Power Electronics* 24, no. 2 (2009): 348–357.

3. R. Sebastian C and P. P. Rajeevan, "Load-Commutated Scr-Based Current Source Inverter Fed Induction Motor Drive With Open-End Stator Windings," *IEEE Transactions on Industrial Electronics* 65, no. 3 (2018): 2031–2038.

4. Z. Wang, B. Wu, D. Xu, and N. R. Zargari, "A Current-Source-Converter-Based High-Power High-Speed Pmsm Drive With 420-Hz Switching Frequency," *IEEE Transactions on Industrial Electronics* 59, no. 7 (2012): 2970–2981.

5. Y. Miao, W. Liao, S. Huang, et al., "DC-Link Current Minimization Scheme for Im Drive System Fed By Bidirectional Dc Chopper-Based CSI," *IEEE Transactions on Transportation Electrification* 9, no. 2 (2023): 2839–2850.

6. G. Migliazza, E. Carfagna, G. Buticchi, F. Immovilli, and E. Lorenzani, "Extended Speed Range Control for A Current Source Inverter Variable Speed Drive," in *IECON 2021–47th Annual Conference of the IEEE Industrial Electronics Society* (IEEE, 2021), 1–6.

7. A. Schiro and S. Oliver, "Wide Bandgap Power to Electrify Our World for A Sustainable Future," *IEEE Power Electronics Magazine* 11, no. 1 (2024): 32–38.

8. V. Madonna, G. Migliazza, P. Giangrande, E. Lorenzani, G. Buticchi, and M. Galea, "The Rebirth of The Current Source Inverter. Advantages for Aerospace Motor Design," *IEEE Industrial Electronics Magazine* 20, no. 4 (2019): 1–15.

9. Z. Huang, T. Yang, P. Giangrande, M. Galea, and P. Wheeler, "Technical Review of Dual Inverter topologies for More Electric Aircraft Applications," *IEEE Transactions on Transportation Electrification* 8, no. 2 (2022): 1966–1980.

10. M. T. Fard, J. He, H. Huang, and Y. Cao, "Aircraft Distributed Electric Propulsion Technologies—A Review," *IEEE Transactions on Transportation Electrification* 8, no. 4 (2022): 4067–4090.

11. J.-S. Lee and U.-M. Choi, "Velocity Profile-Based Evaluation and Improvement of Lifetime of Power Devices In Railway Propulsion Inverters," *IEEE Journal of Emerging and Selected Topics in Power Electronics* 10, no. 2 (2022): 1384–1394.

12. C. Lyu and V. Dinavahi, "Zero-Emission Marine Vessels: Multidomain Modeling and Real-Time Hardware-In-The-Loop Emulation On Adaptive Compute Acceleration Platform," *IEEE Electrification Magazine* 11, no. 4 (2023): 54–63.

13. P. Niedermayr, L. Alberti, S. Bolognani, and R. Abl, "Implementation and Experimental Validation of Ultrahigh-Speed Pmsm Sensorless Control By Means of Extended Kalman Filter," *IEEE Journal of Emerging and Selected topics in Power Electronics* 10, no. 3 (2022): 3337–3344.

14. E. P. Wiechmann, P. Aqueveque, R. Burgos, and J. Rodriguez, "On The Efficiency of Voltage Source and Current Source Inverters for High-Power Drives," *IEEE Transactions on Industrial Electronics* 55, no. 4 (2008): 1771–1782.

15. G. L. Fidone, G. Migliazza, E. Carfagna, et al., "Common Architectures and Devices for Current Source Inverter In Motor-Drive Applications: A Comprehensive Review," *Energies* 16, no. 15 (2023): 5645.

16. G. Migliazza, G. Buticchi, E. Carfagna, et al., "DC Current Control for A Single-Stage Current Source Inverter In Motor Drive Application," *IEEE Transactions on Power Electronics* 36, no. 3 (2021): 3367–3376.

17. D. Benatti, G. Migliazza, E. Carfagna, F. Immovilli, and E. Lorenzani, "Novel Single-Stage Current Source Inverter: Extension to Low-Speed Region In Motor Drive Applications," *IEEE Transactions on Industrial Electronics* 71, no. 9 (2024): 10335–10345.

18. J. Liu and Y. Zhang, "Performance Improvement of Nonlinear Flux Observer for Sensorless Control of PMSM," *IEEE Transactions on Industrial Electronics* 70, no. 12 (2023): 12 014–12 023.

19. S. Bolognani, S. Calligaro, and R. Petrella, "Design Issues and Estimation Errors Analysis of Back-Emf-Based Position and Speed Observer for Spm Synchronous Motors," *IEEE Journal of Emerging and Selected topics in Power Electronics* 2, no. 2 (2014): 159–170.

20. H. Yang, A. Xu, Y. Zhang, and X. Chai, "Error Analysis and Design of Sliding-Mode-Observer-Based Sensorless PMSM Drives Under A Low Sampling Ratio," *IEEE Transactions on Power Electronics* 39, no. 7 (2024): 7783–7792.

21. A. Ding, Z. Sun, C. Huang, W. Xu, and Y. Mao, "Position Sensorless Control of A Dual Three-Phase Pmlsm for Electromagnetic Launch Based On The Linear Quadratic Regulator and Kalman Filter," *IEEE Transactions on Industrial Electronics* 71, no. 8 (2024): 8383–8394.

22. E. Al-nabi, B. Wu, N. R. Zargari, and V. Sood, "Sensorless Control of CSC-fed IPM Machine for Zero- and Low-Speed Operations Using Pulsating HFI Method," *IEEE Transactions on Industrial Electronics* 60, no. 5 (2013): 1711–1723.

23. D. Basic, F. Malrait, and P. Rouchon, "Current Controller for Low-Frequency Signal Injection and Rotor Flux Position Tracking At Low Speeds," *IEEE Transactions on Industrial Electronics* 58, no. 9 (2011): 4010–4022.

24. R. A. torres, S. Lee, H. Dai, W. Lee, T. M. Jahns, and B. Sarlioglu, "Analysis of Pulsating High-Frequency Injection Self-Sensing Control for CSI PM Motor Drives," *IEEE Transactions on Power Electronics* 40, no. 3 (2025): 4345–4357.

25. Z. Zhang and J. Lamb, "Active Q Flux Concept for Sensorless Control of Synchronous Reluctance Machines," *IEEE Transactions on Industrial Electronics* 70, no. 5 (2023): 4526–4536.

26. L. Ding, Y. W. Li, and N. R. Zargari, "Discrete-time SMO Sensorless Control of Current Source Converter-Fed PMSM Drives With Low Switching Frequency," *IEEE Transactions on Industrial Electronics* 68, no. 3 (2021): 2120–2129.

27. L. Ding, Y. W. Li, N. R. Zargari, and R. Paes, "Sensorless Control of CSC-fed PMSM Drives With Low Switching Frequency for Electrical Submersible Pump Application," *IEEE Transactions on Industry Applications* 56, no. 4 (2020): 3799–3808.

28. A. K. Abdelsalam, M. I. Masoud, M. S. Hamad, and B. W. Williams, "Improved Sensorless Operation of a CSI-based Induction Motor Drive: Long Feeder Case," *IEEE Transactions on Power Electronics* 28, no. 8 (2013): 4001–4012.

29. M. Bahrami-Fard, M. G. Korrani, M. Rastegar, and B. Fahimi, "Advanced Startup and Smooth Transition to Sensorless Field Oriented Control for CSI-fed PMSM Drives In Submersible Pumps," *IEEE Transactions on Power Electronics* 40, no. 9 (2025): 12 402–12 415.

30. R. A. Torres, H. Dai, W. Lee, T. M. Jahns, and B. Sarlioglu, "Evaluation of Sensorless Techniques for Surface Permanent-Magnet Integrated Motor Drive Using Current-Source Inverter," in *2020 IEEE Energy Conversion Congress and Exposition (ECCE)* (IEEE, 2020), 2387–2394.

31. T. Boileau, N. Leboeuf, B. Nahid-Mobarakeh, and F. Meibody-Tabar, "Online Identification of PMSM Parameters: Parameter Identifiability and Estimator Comparative Study," *IEEE Transactions on Industry Applications* 47, no. 4 (2011): 1944–1957.

32. T. Wang, J. Huang, M. Ye, et al., "An EMF Observer for PMSM Sensorless Drives Adaptive to Stator Resistance and Rotor Flux Linkage," *IEEE Journal of Emerging and Selected Topics in Power Electronics* 7, no. 3 (2019): 1899–1913.

33. Y. Yao, Y. Huang, F. Peng, and J. Dong, "Position Sensorless Drive and Online Parameter Estimation for Surface-Mounted Pmsms Based On Adaptive Full-State Feedback Control," *IEEE Transactions on Power Electronics* 35, no. 7 (2020): 7341–7355.

34. Y. Yu, X. Huang, Z. Li, et al., "Full Parameter Estimation for Permanent Magnet Synchronous Motors," *IEEE Transactions on Industrial Electronics* 69, no. 5 (2022): 4376–4386.

35. Y. Yu, X. Huang, and Z. Li, "Overall Electrical Parameters Identification for Ipmsms Using Current Derivative to Avoid Rank Deficiency," *IEEE Transactions on Industrial Electronics* 70, no. 7 (2023): 7515–7520.

36. E. Carfagna, G. Migliazza, G. Buticchi, et al., "Pll-Based Sensorless Control for Single-Stage Current Source Inverter In Motor Drive Application," in *IECON 2021–47th Annual Conference of the IEEE Industrial Electronics Society* (IEEE, 2021), 1–6.

37. J. Zhang, F. Peng, Y. Huang, Y. Yao, and Z. Zhu, "Online Inductance Identification Using PWM Current Ripple for Position Sensorless Drive of High-Speed SPMSM," *IEEE Transactions on Industrial Electronics* 69, no. 12 (2022): 12426–12436.

38. G. Buticchi, E. Lorenzani, F. Immovilli, and C. Bianchini, "Active Rectifier With Integrated System Control for Microwind Power Systems," *IEEE Transactions on Sustainable Energy* 6, no. 1 (2015): 60–69.

39. E. Carfagna, C. M. Verrelli, G. Migliazza, F. Bernardi, and E. Lorenzani, "Stator Flux Observers for Speed-Controlled PMSMs in Low-Speed Sensorless Applications: Comparative Tests and Hybrid Strategy," *IEEE Transactions on Control Systems Technology* 33, no. 5 (2025): 1905–1912.

40. A. Bendre, I. Wallace, J. Nord, and G. Venkataramanan, "A Current Source PWM Inverter With Actively Commutated SCRs," *IEEE Transactions on Power Electronics* 17, no. 4 (2002): 461–468.

41. A. R. Beig and V. T. Ranganathan, "A novel CSI-fed induction motor drive," *IEEE Transactions on Power Electronics* 21, no. 4 (2006): 1073–1082.

42. R. Teodorescu, M. Liserre, and P. Rodriguez, *Grid Converters for Photovoltaic and Wind Power Systems* (John Wiley & Sons, 2011).